



Title	Recycling of calcined carbonated cement pastes as cementitious materials: Proposed CCUS technology for calcium looping
Author(s)	Kong, Y. K.; Ruan, S.; Kurumisawa, Kiyofumi
Citation	Journal of environmental chemical engineering, 10(5), 108247 https://doi.org/10.1016/j.jece.2022.108247
Issue Date	2022-10
Doc URL	http://hdl.handle.net/2115/92727
Rights	© <2022>. This manuscript version is made available under the CC-BY-NC-ND 4.0 license http://creativecommons.org/licenses/by-nc-nd/4.0/
Rights(URL)	http://creativecommons.org/licenses/by-nc-nd/4.0/
Type	article (author version)
File Information	PAPYK202103-1__clean_version_.pdf



[Instructions for use](#)

Recycling of calcined carbonated cement pastes as cementitious materials:

Proposed CCUS technology for calcium looping

Y.K. Kong ^{a,b}, S.Ruan ^b, Kiyofumi Kurumisawa ^{c*}

^a Division of Sustainable Resources Engineering, Graduate School of Engineering,

Hokkaido University, Japan

^b College of Civil Engineering and Architecture, Zhejiang University, Hangzhou

310058, China

^c Division of Sustainable Resources Engineering, Faculty of Engineering, Hokkaido

University, Japan

Abstract: In this study, calcined carbonated hydrated cement pastes (HCPs) were used to partially replace ordinary Portland cement (OPC) as a cementitious material. Calcined HCP can be derived from carbonated HCP after the release of CO₂ for the carbon capture, utilization, and storage (CCUS). Calcined carbonated HCP was produced by calcining carbonated HCP at 1000 °C, also used in calcium looping. The crystal phase compositions of the HCP, carbonated HCP, and calcined carbonated HCP were identified. Various hardening and microstructural tests on the composite cement paste mixtures blended with calcined carbonated HCP were performed. The initial results showed that the HCP could sequester CO₂, forming various calcium carbonates.

*Kiyofumi Kurumisawa (kurumi@eng.hokudai.ac.jp, corresponding author); Y.K. Kong (ykkong@elms.hokudai.ac.jp); S. Ruan (sruan001@zju.edu.cn).

21 After carbonated HCP calcination, the main nanocrystalline phases of calcium silicate
22 hydrate (C-S-H) and calcium carbonate decomposed, forming lime and wollastonite.
23 The 28-day compressive strength of the calcined carbonated HCP–OPC mixtures
24 increased with the replacement ratio up to 20%, owing to the filler effect of wollastonite.
25 The microstructural analysis revealed that the portlandite, C-S-H, and
26 monocarboaluminate phases were formed after hydration. Finally, by recycling
27 demolition waste, this study proposed a technology roadmap for CCUS to achieve this
28 goal, and a life cycle assessment was conducted to evaluate and compare the
29 environmental impacts of producing 1 t of calcined carbonated HCP–OPC mixtures and
30 plain OPC paste.

31

32 **Keywords:** Carbon capture, utilization, and storage; Calcium looping; Calcined
33 carbonated cement paste; Compressive strength; Microstructural analysis; Life cycle
34 assessment.

35 **1. Introduction**

36

37 Continuous greenhouse gas emissions from human activities have been one of the
38 most severe environmental problems for decades [1]. Greenhouse gases are mainly
39 emitted by industries, of which cement production generates a large volume of CO₂
40 emissions. [1]. The industrial sector that manufactures ordinary Portland cement (OPC)
41 generates approximately 5%–9% of the total CO₂ anthropogenic emissions [2] [3]. If
42 greenhouse gas emissions are not controlled or mitigated, product proliferation will
43 pose a significant threat to the ecosystem [4].

44 The two main methods used to reduce CO₂ emissions during concrete production
45 are (1) decreasing the amount of cement produced and (2) capturing the emitted CO₂
46 within the life cycle of concrete structures [5] [6]. Conventionally, supplementary
47 cementitious materials (SCMs) such as fly ash and granulated ground blast-furnace slag
48 are utilized to partially or wholly replace OPC in concrete [7] [8]. Although SCMs are
49 faced with reaching global limits, the demand for OPC is continuously increasing [5].
50 Another approach to decreasing the total CO₂ emissions of concrete structures is
51 through carbon capture, utilization, and storage (CCUS), characterized by sustainability
52 and energy savings [9]. CCUS is the process of reducing the CO₂ volume and achieving
53 benefits by converting CO₂ into high-value products for different industries [9] [10]. In
54 the past, CO₂ was sequestered in silica-rich natural rocks [6]. However, the demand for
55 silicate rocks is very high, owing to the large volume of emitted CO₂ [11]. It is estimated
56 that to sequester 1 t of CO₂, approximately 1.6–3.7 t of carbonatable materials are

57 required, depending on the CO₂ uptake capacity of the materials used [6]. In addition,
58 the associated mining activities and transportation of natural rocks for carbonation can
59 cause significant environmental impacts. To address these limitations, researchers have
60 focused on using demolished concrete structures to replace natural rocks [12] [13].

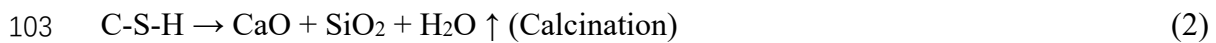
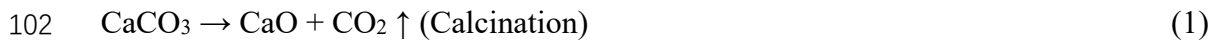
61 The use of demolished concrete, characterized by its high alkalinity and abundant
62 Ca²⁺ content, to capture CO₂ has become prevalent in recent years [14] [9]. Unlike the
63 limited natural rock resources, an estimated 900 Mt of demolished concrete is generated
64 annually in Europe, the U.S., and Japan [15]. The components of demolished concrete
65 include aggregates and fully hydrated cement paste (HCP), which is rich in portlandite
66 (Ca(OH)₂) and can sequester CO₂ [16] [17]. For demolished concrete, portlandite in
67 HCP should be carbonated. However, because of the initially formed calcium carbonate
68 at the surface of the concrete structure, further carbonation can be prevented by these
69 carbonate products, indicating that the inner portlandite is still not consumed [18] [19].
70 The carbonation of HCP commences with the penetration of CO₂ into the cement matrix,
71 which dissolves in the pore solution to form CO₃²⁻ ions [12]. These two ions react with
72 portlandite and calcium silicate hydrate (C-S-H), forming various calcium carbonates,
73 such as calcite, vaterite, aragonite, silica gel, and hydrated iron oxides [20] [21].
74 Adopting HCP from construction waste to capture CO₂ can recycle demolished concrete
75 and produce carbonated cement paste with a significant value. Some researchers have
76 revealed the pozzolanic reactivity of carbonated HCP powders, reporting that they can
77 be utilized as SCMs to partially replace OPC in concrete mixtures [22]. However, the

78 properties of carbonated HCP after CO₂ release through calcination have not been
79 investigated in detail.

80 Numerous studies on using recycled concrete to sequester CO₂ have been
81 conducted; most studies focused on the CO₂ capture efficiency of HCP, phase
82 assemblage of HCP after carbonation, and cementitious properties of HCP carbonation
83 [23] [24] [19]. However, a significant aspect of CCUS is the release and reuse of stored
84 (almost pure) CO₂ to manufacture valuable bioproducts [9] [10], which has been
85 neglected by researchers in civil engineering. As mentioned above, the main phase of
86 sequestered CO₂ in HCP carbonation is calcium carbonate (CaCO₃). Currently, the
87 conventional method for decomposing CaCO₃ is calcination [25]. This approach has
88 been introduced in the thermochemical energy storage system, which relies on the
89 carbonation–calcination reaction of CaCO₃/CaO, known as calcium looping (CaL) [26]
90 [27]. For CaL, calcium carbonates are typically derived from natural resources, such as
91 natural limestone and dolomite. Combining CCUS technology with construction and
92 demolition waste to capture CO₂ to generate CaCO₃ is more sustainable than collecting
93 natural limestone [27]. Moreover, the traditional CaL requires somewhat high
94 temperatures to convert CaO into CaCO₃. The calcination of CaCO₃ may still be energy-
95 consuming for CaCO₃ decomposition to release CO₂, requiring a temperature range of
96 919–1199 °C (1193–1473 K). Under H₂O steaming conditions, the decomposition
97 temperature can be decreased to 899 °C (1173 K) compared to the direct calcination by
98 combusting fossil fuels [28]. The calcination of carbonated HCP decomposes various

99 calcium carbonates and the remaining noncarbonated C-S-H when the temperature
100 reaches 700–900 °C, as expressed by Equations (1) and (2) [29].

101



104

105 Calcium oxide (CaO) and silica (SiO₂) are cementitious components produced after
106 the calcination of carbonated HCP. CaO is the major chemical oxide in lime that
107 improves the early-age strength of concrete [30], and SiO₂ is highly rich in silica fume,
108 which exhibits strong pozzolanic reactivity and can refine the pore structure of hardened
109 pastes [31]. Lime and silica fume are extensively utilized in construction [30] [32] [33].
110 Barbhuiya et al. [34] reported that the early-age compressive strength of fly-ash-based
111 concrete could be improved by adding hydrated lime and silica fume. Das et al. [30]
112 observed that fly-ash-based geopolymer concrete attained the highest compressive
113 strength when 7.5% and 2.0% fly ash were replaced with lime and silica fume,
114 respectively. Calcination of carbonated HCP may be the best approach to releasing and
115 utilizing captured CO₂. In a previous study, the authors developed a CO₂ sponge
116 through HCP calcination to recapture CO₂ under saturation conditions. A technology
117 roadmap for recycling HCP, carbonated HCP, and calcined HCP in CCUS was plotted,
118 as reported in Ref. [35]. Therefore, in the previous study, the authors achieved CaL by
119 recycling HCP from demolition waste to repeatedly sequester and release CO₂. In this
120 study, the cementitious potential of calcined carbonated HCP was investigated to extend

121 and complete the entire recycling cycle of CCUS using HCP. If the cementing effects
122 of calcined carbonated HCP are revealed, CaL products will not be limited to the form
123 of storage media for CO₂.

124 Therefore, the extensive use of calcined carbonated HCP is proposed, and a novel
125 approach for CCUS can be developed. Previous studies mainly focused on the seeding
126 effect and SCM-like properties of carbonated HCP powders during the hydration of
127 OPC-based mixtures containing carbonated HCP powders [36]. Moreover, the disposal
128 of by-products generated from CO₂-released carbonated HCP has not been investigated
129 extensively. In this study, calcined carbonated HCP was systematically investigated, in
130 which HCP underwent carbonation and calcination. The cementing effects of the
131 calcined carbonated HCP were evaluated through macro- and micro-structural
132 evaluations. Moreover, a life cycle assessment for evaluating environmental impacts
133 during the production of calcined carbonated HCP–OPC mixtures was conducted. It is
134 believed that this study will facilitate the development of CCUS for practical
135 applications.

136

137 **2. Experimental program**

138

139 2.1. Materials and preparation of specimens

140 2.1.1. Preparation of HCP, carbonated HCP, and calcined carbonated HCP

141 Before preparing carbonated HCP, HCP was manufactured using Type CEM I OPC
142 with a strength class of 42.5 N, complying with ASTM C150 [37]. In actual construction

143 work, HCP can be obtained from demolished concrete using comminution and magnetic
144 methods, which are advanced techniques for producing recycled aggregate concrete [38]
145 [39]. HCP specimens were cast in 100 mm × 100 mm × 100 mm molds with a constant
146 water-to-cementitious material (W/CM) ratio of 0.5, according to ASTM C305
147 requirements [40]. The hardened specimens were cured at 23±0.5 °C and relative
148 humidity of 100%. After curing for one day, the HCP samples were demolded and
149 hydrated at 60±0.5 °C for 90 days, accelerating hydration to simulate the OPC paste
150 derived from demolition waste, consistent with Skocek et al. [6]. The hydration degree
151 of the clinker was close to 90% (not 100%) under the above curing conditions.
152 Moreover, a curing temperature of 60±0.5 °C would not significantly change the
153 microstructure of the cement paste but could accelerate the hydration process [41]. The
154 HCP specimens were then pulverized into 75 μm powders by ball milling and
155 carbonated for 24 h to produce carbonated HCP; the carbonation was conducted in an
156 autoclave, providing a pure CO₂ environment (99.9%) with a constant gas pressure of
157 1.5 MPa. Most recent studies on CaL have been focused on carbonation under low CO₂
158 partial pressure, indicating that low CO₂ concentrations in the flue gas in the power
159 plant were used. However, for thermochemical energy storage in the CaL to sequester
160 CO₂, a high CO₂ concentration (pure CO₂ environment) is required [26]. The
161 carbonation autoclave set can be found in Refs. [35] [42]. The weight differences before
162 and after carbonation were measured. After each carbonated HCP specimen cooled
163 down to room temperature, it was calcined in a muffle furnace to produce calcined
164 carbonated HCP. The initial temperature was 30 °C, which was increased to 1000 °C at

165 a constant heating rate of 4 °C/min. The final temperature (1000 °C) was maintained
166 for 2 h to completely decompose calcium carbonate. This calcination temperature range
167 was consistent with our previous study, and the decomposition products of calcium
168 carbonates were obtained [35]. After calcination, the calcined carbonated HCP was
169 removed and weighed.

170

171 2.1.2. Preparation of composite cement paste

172 Composite cement pastes were prepared using Type CEM I with a strength class of
173 42.5 N, OPC-calcined carbonated HCP, and tap water. The chemical compositions of
174 OPC were determined using X-ray fluorescence spectrometry (XRF), as listed in Table
175 1. Four groups of paste mixtures were produced and subjected to tests to evaluate the
176 influence of HCP calcination on the properties of the OPC pastes. Specifically, they
177 comprised three groups of OPC pastes partially replaced with calcined carbonated HCP
178 (calcined carbonated HCP–OPC pastes) and one group of plain OPC pastes as the
179 reference (Ref.). For consistency, the W/CM ratio was maintained at 0.40 for all the
180 mixtures. The mixing proportions are listed in Table 2. For clarity, each experimental
181 group was labelled “MN,” where N denotes the replacement ratio of calcined
182 carbonated HCP in the binder, ranging from 10% to 30%.

183 A Hobart mixer was used to produce paste mixtures according to ASTM C305, and
184 the mixtures were cast in 20 mm × 20 mm × 20 mm molds. Immediately after casting,
185 the fresh paste mixtures were placed on a vibration table and compacted until no visible
186 bubbles appeared on the surfaces of the samples. Next, the samples were covered by a

187 thin cling film and cured at 23 ± 0.5 °C for 24 h. After curing for one day, the samples
188 were demolded and immersed in a water tank at 23 ± 0.5 °C to prevent drying shrinkage.

189

190 2.2. Test methods

191 2.2.1. Compressive strength

192 A hydraulic compression machine was used to determine the 28-day compressive
193 strength of the specimens according to ASTM C109 [43]. The test results for each
194 mixture were calculated as the average strength of triplicate specimens.

195

196 2.2.2. X-ray diffraction (XRD)

197 XRD was conducted to investigate the phase formations of the paste samples.
198 Before the XRD test, the paste samples were crushed and oven-dried for one day.
199 Subsequently, the crushed samples were milled to fine powders (≤ 75 μm) before the
200 XRD tests. XRD patterns were analyzed using an XRD Bruker D8 Advance instrument.
201 The $\text{CuK}\alpha$ X-ray ($\lambda = 1.5418$ Å) was generated at 40 mA and 40 kV. Scanning
202 measurements were conducted within a 2θ range from 5° to 90° in a step size of 0.02° .

203

204 2.2.3. Thermogravimetric analysis (TGA)

205 For parallel comparison, milled fine-sized powders of approximately 5.0 mg were
206 used to conduct TGA using a Mettler Toledo STARe System TGA2. The powders were
207 heated from 30 °C up to 1000 °C in open vessels in an N_2 atmosphere at a heating rate

208 of 15 °C/min. The thermogravimetric (TG) and derivative thermogravimetric (DTG)
209 curves of the paste samples were plotted.

210

211 2.2.4. Fourier-transform infrared spectroscopy (FTIR)

212 A Nicolet iS50 FTIR spectrometer with a frequency range of 4000–400 cm⁻¹ at a 4
213 cm⁻¹ resolution was used to obtain the FTIR data of the specimens. Thirty-two scans
214 were recorded for each sample. KBr discs were prepared by pressing pellets composed
215 of the samples and KBr at a ratio of 1:100.

216

217 **3. Results and discussion**

218

219 3.1. Before mixing

220 3.1.1. Weight variations in HCP after carbonation and calcination

221 Table 3 lists the content for each processing procedure and the weight change ratio
222 after each processing step. A weight increase in HCP was observed after carbonation
223 with an increase ratio of 21.25% because CO₂ was sequestered. A decrease in weight
224 was observed when the carbonated HCP was calcined at 1000 °C. This weight decrease
225 could be attributed to the decomposition of specific phases within the carbonated HCP,
226 and the phases should contain various types of calcium carbonates. The weight decrease
227 ratio of 35.35% was higher than the above weight increase ratio, indicating that other
228 phases other than calcium carbonates decomposed, as discussed later.

229

230 3.1.2. XRD patterns

231 Fig. 1 shows the XRD patterns of the HCP, carbonated HCP, and calcined
232 carbonated HCP. Various hydration products, that is, portlandite ($2\theta = 18.0^\circ, 34.2^\circ,$
233 $47.1^\circ, 54.4^\circ,$ and 62.6°), C-S-H ($2\theta = 26.5^\circ$ and 29.3°), and monocarboaluminate phases,
234 $C_4\bar{A}CH_{11}$ ($2\theta = 11.6^\circ$), were observed in the HCP [22] [44] [45]. In addition, a slight
235 peak was detected at $2\theta = 39.3^\circ$, which was attributed to calcite formed by natural
236 carbonation. The presence of calcite leads to the formation of monocarboaluminate [46].
237 Compared to the HCP, a significant decrease in the intensity of portlandite was detected
238 in the carbonated HCP. In contrast, a conspicuous appearance of calcium carbonate was
239 observed at $2\theta = 23.0^\circ, 29.4^\circ, 32.5^\circ, 39.3^\circ, 43.2^\circ, 45.9^\circ,$ and 48.5° , indicating that HCP
240 carbonation consumed the most portlandite, forming various calcium carbonates [47].
241 The C-S-H did not appear to be significantly carbonated during HCP carbonation,
242 which might be attributed to the preformed calcite layer preventing further C-S-H
243 carbonation [48] [49]. Regarding the calcined carbonated HCP, the crystal phases of
244 calcium carbonates and nanocrystalline phases of C-S-H mentioned above almost
245 vanished [50], whereas CaO was detected ($2\theta = 37.3^\circ$), corresponding to the C-S-H
246 decomposition expressed by Equation (2). Moreover, wollastonite ($CaSiO_3$) was
247 detected at peaks of $23.1^\circ, 32.0^\circ, 41.2^\circ,$ and 44.8° and a continuous zig-zag pattern of
248 $55^\circ\text{--}60^\circ$ [51] [52] [53]. As expressed by Equations (1) and (2), calcination decomposes
249 calcium carbonates and C-S-H, releasing CO_2 and evaporated H_2O [51]. Calcination
250 could also release pore solutions and gel water, which explains why the weight decrease
251 ratio after calcination exceeded the weight increase ratio after carbonation. Furthermore,

252 the lime and quartz could react in the muffle forming wollastonite at high temperatures
253 up to 1000 °C, owing to the decomposition of C-S-H and calcite, as expressed by
254 Equation (3) [54].

255



257

258 3.1.3. TG-DTG curves

259 Fig. 2 shows the TGA results for the HCP, carbonated HCP, and calcined
260 carbonated HCP, consistent with the XRD results. The DTG curves for the three
261 different samples varied significantly, suggesting the formation of different products in
262 the HCP after carbonation and calcination. When the temperature increased from 30 to
263 150 °C, the nanocrystalline phases of C-S-H in the HCP and carbonated HCP
264 dehydrated, indicating that C-S-H essentially remained noncarbonated [13]. However,
265 no weight decrease was observed in the calcined carbonated HCP, possibly owing to
266 hydrated product decomposition caused by calcination. As the temperature increased to
267 400–450 °C, a significant weight decrease was detected in the HCP, attributed to
268 portlandite decomposition [55]; in contrast, the carbonated HCP underwent a slight
269 weight decrease, suggesting that a small portion of the portlandite was noncarbonated.
270 A low and broad maximum appeared on the DTG curve of the calcined carbonated HCP
271 at approximately 400 °C, which should correspond to portlandite decomposition in
272 agreement with the XRD patterns [56]. When heating temperature continued increasing
273 to 800 °C, a broad and high peak occurred in the carbonated HCP because of the

274 decarbonation of the calcium carbonates. However, a broad and short peak appeared in
275 the HCP curve, attributed to the weak natural carbonation of HCP within its long curing
276 period [49]. Based on the TG results, the CO₂ uptake ratio was calculated using the
277 weight loss difference of the carbonated HCP and calcined carbonated HCP at 500–
278 900 °C, which was 21.61%. This value is close to the weight increase ratio of the HCP
279 after carbonation, indicating that weight gain is generally associated with CO₂
280 sequestration. It was difficult to observe the weight variation in the calcined carbonated
281 HCP at high temperatures (above 900 °C), demonstrating that CO₂ was entirely released
282 during calcination.

283

284 3.2. After producing composite cement paste

285 3.2.1. Compressive strength

286 The 28-day compressive strength results for each paste mixture were determined
287 (Fig. 3) to evaluate the influence of HCP calcination on the mechanical properties of
288 the OPC pastes. Overall, the compressive strength first increased with increasing
289 replacement ratio and then decreased. The reference group specimen exhibited a 28-
290 day compressive strength of 37.8 MPa. The compressive strength values of M10 and
291 M20 were higher than that of the reference group, but the compressive strength of M30
292 decreased significantly. Thus, the strength of the paste mixture increased when the
293 calcined carbonated HCP replacement ratio increased from 0% to 20%, beyond which
294 the strength development of the paste was significantly hindered. Therefore, an
295 optimum calcined carbonated HCP replacement ratio of 20% improved the compressive

296 strength by up to 8%. The strength improvement caused by HCP calcination might be
297 attributed to the effect of wollastonite. Previous studies have investigated the possibility
298 of mixing ground wollastonite powder in cement pastes and revealed the cementitious
299 properties of wollastonite [52]. Wahab et al. [57] found that using wollastonite to
300 replace 20% sand could improve the mechanical properties of mortar mixtures. Kalla
301 et al. [58] observed that when 10%–15% of cement was replaced with wollastonite, the
302 permeability and chloride diffusion coefficients of concrete mixtures decreased. Both
303 studies reported an optimum ratio of 20% for using wollastonite to replace other
304 construction materials, consistent with the compressive strength results. The beneficial
305 effect of wollastonite on hydration behavior can be attributed to the filler effect and
306 reduced heat generation [53] [52]. The surface areas of finer wollastonite provide
307 additional nucleation sites for C-S-H growth [59]. However, with a slight increase in
308 the replacement ratio, the dilution effect caused by the calcined carbonated HCP may
309 decrease the strength of the paste mixtures [60]. Hence, it is possible to utilize calcined
310 carbonated HCP to partially replace cement at the optimum content, maintaining the
311 same or improved mechanical properties.

312

313 3.2.2. XRD

314 Fig. 4 shows the XRD patterns of the paste mixtures after curing for 28 days.
315 Common hydration products, including portlandite, C-S-H, and monocarboaluminate,
316 were detected in all the groups. A low and narrow peak at $2\theta = 39.3^\circ$ was observed,
317 related to atmospheric carbonation during curing and measurements. No significant

318 differences between the M10, M20, and reference groups were observed. However, a
319 sharp peak with a significantly high portlandite intensity ($2\theta = 18.0^\circ$) was observed in
320 M30, owing to the high replacement ratio of calcined carbonated HCP containing a
321 comparatively larger amount of CaO, which reacted with H₂O to form portlandite.
322 Moreover, the C-S-H intensity at $2\theta = 29.3^\circ$ was lower than that of the reference group,
323 probably because the higher calcined carbonated HCP content diluted the clinker [60].
324 The XRD results are consistent with the compressive strength results. The calcined
325 carbonated HCP increased the strength, although the degree of improvement was
326 insignificant. Moreover, the XRD patterns of the Ref., M10, and M20 groups were
327 similar. A significant decrease in the compressive strength of M30 was observed from
328 the XRD patterns, with a significantly higher portlandite intensity and lower C-S-H
329 intensity than those of the other groups.

330

331 3.2.3. TGA

332 Fig. 5 shows the DTG and TG curves of the paste mixtures. The TGA results were
333 consistent with the XRD patterns and compressive strength measurements. Three main
334 decomposition steps were observed in the DTG curves in agreement with previous
335 findings [13] [55] [56] [31], identified as follows:

336 (1) 30–300 °C: Dehydration of water bonded to C-S-H.

337 (2) 300–500 °C: Decomposition of portlandite.

338 (3) 500 – 900 °C: Decarbonation of various calcium carbonates, including
339 amorphous calcium carbonates, vaterite, aragonite, and calcite.

340 The weight loss percentages of the paste mixtures associated with the water and CO₂
341 contents are listed in Table 4. The carbonation degree, represented by amorphous
342 calcium carbonates (~650 °C), was also reflected. A minimal difference in weight loss
343 was observed for all the paste mixtures, consistent with the similar XRD patterns among
344 the reference and experimental groups. Moreover, the total weight loss of the
345 experimental groups increased with an increase in the calcined carbonated HCP content,
346 attributed to the increased portlandite content. A similar total weight loss of
347 approximately 21% revealed by these mixtures was consistent with the 28-day
348 compressive strength results, indicating a relationship between the extent of hydration
349 and the mechanical properties [13].

350

351 3.2.4. FTIR

352 Fig. 6 shows the FTIR spectra of the OPC pastes containing partially replaced
353 calcined carbonated HCP after curing for 28 days. No significant differences among the
354 four groups of paste mixtures were observed, consistent with the XRD patterns and TG-
355 DTG curves. Six major bands were observed in all the specimens. First, a sharp
356 absorption at 3644 cm⁻¹ was detected, associated with the symmetrical stretching
357 vibration of hydroxyl groups [61]. A wide band at a wavenumber of approximately 3500
358 cm⁻¹ revealed the existence of portlandite in the reference and experimental groups [62].
359 All the specimens showed a narrow absorption band at wavenumbers of 1500–1750 cm⁻¹
360 ¹, corresponding to the water content (for example, gel water) in the cement matrix.
361 Subsequently, a significant band at approximately 1450 cm⁻¹ was detected, owing to the

362 ν_2 bending vibration of C-O [61]. As mentioned earlier, the existence of C-O was
363 attributed to natural carbonation, in agreement with the TGA results. A broad absorption
364 band was observed at approximately 970 cm^{-1} , associated with the Si-O in-plane
365 stretching vibration of the Q₂ tetrahedra in C-S-H gels [63]. No distinct shifts in the
366 wavenumber of Si-O stretching bands were observed for the reference and experimental
367 groups. This indicates that an increased replacement ratio of calcined carbonated HCP
368 in the binder system would not significantly influence Si polymerization, consistent
369 with the characterization and mechanical test results.

370

371 **4. Further discussion**

372 Consistent with previous findings [22] [16] [64], the ability of HCP to sequester
373 CO₂ leads to the formation of carbonated HCP. After the calcination of carbonated HCP,
374 the crystal phases of portlandite, C-S-H, and calcium carbonates decomposed, and new
375 phases of lime and wollastonite were formed. With dehydration and decarbonation,
376 water and CO₂ were released, generating the discrepancy between the weight increase
377 in HCP after carbonation and the weight decrease in carbonated HCP after calcination.
378 Furthermore, the mechanical properties of the OPC pastes partially replaced with
379 calcined carbonated HCP were consistent with the hydration degree. Facilitated by
380 microscopic investigations, the hydration behaviors of the calcined carbonated HCP–
381 OPC pastes are discussed below.

382

383 4.1. Hydration behaviors of calcined carbonated HCP–OPC paste mixtures

384 Based on the detailed investigation of Ref., M10, M20, and M30, the hydration
385 mechanism of the calcined carbonated HCP–OPC paste mixtures is evident. Fig. 7
386 depicts the underlying mechanisms of the hydration behavior. Based on the mechanical
387 and microscopic test results, the cementing effect of calcined carbonated HCP was
388 observed, owing to the presence of lime, silica, and wollastonite, which were formed
389 from the dehydrated C-S-H, portlandite, and decarbonated calcium carbonates. After
390 mixing, the added wollastonite in the calcined carbonated HCP provided nucleation
391 sites for cement hydration, favoring C-S-H growth. In addition, silica reacted with
392 $\text{Ca}(\text{OH})_2$ -rich pore solutions to generate additional C-S-H, improving the compressive
393 strength [65]. The slight improvement in the 28-day compressive strength might also
394 be influenced by the filling effect of wollastonite, leading to pore densification.
395 Furthermore, the dilution effect of the calcined carbonated HCP should be considered,
396 as wollastonite did not contribute to the strength gain. Because of these two contrasting
397 effects on cement hydration, an optimum replacement ratio (20%) of calcined
398 carbonated HCP existed in the binder system, at which the strength enhancement effect
399 could compensate for the dilution effect. Above this optimum replacement ratio, the
400 dilution effect was the dominant mechanism, and the mechanical properties of the
401 composite cement pastes decreased significantly. Moreover, a higher amount of
402 calcined carbonated HCP produced a higher portlandite content, which might cover the
403 calcium silicate surface and prevent further hydration.

404

405 4.2. Proposed CCUS technology routine

406 Regarding the cementing effect of calcined carbonated HCP, recycling carbonated
407 HCPs in CCUS is feasible. Fig. 8 shows a technology roadmap of CCUS using
408 demolished concrete structures. During this process, CO₂ undergoes five stages: 1)
409 emission from the concrete structure, 2) capture by HCP, 3) transportation, 4)
410 calcination for release, and 5) reuse. CCUS starts from the assumed 1 t of CO₂ emitted
411 during the production and demolition of concrete structures. According to the
412 Intergovernmental Panel on Climate Change [66], CO₂ can be generated within the
413 entire life cycle of a concrete structure, from concrete production to the demolition of
414 the structure, as shown by the rectangle plotted by the dashed line in the roadmap. The
415 total amount of HCP used was 1000 kg. The CO₂ flow was quantitatively evaluated in
416 each step, and the CO₂ sequestering and release ratios were based on the experimental
417 results of this study. After demolition, concrete waste can be sorted into aggregates and
418 HCP. The aggregates can be used as recycled aggregates for producing new concrete,
419 and the HCP can be used as the sequestering media for the emitted CO₂ during the
420 service life of the concrete structure. A total of 210 kg of CO₂ was captured in the HCP
421 as the formed calcium carbonates in the first recycling phase and transported (for
422 example, using a lorry) without pipeline networks, significantly decreasing the energy
423 penalty [11]. Carbonated HCP can be calcined to release CO₂, which can be further
424 dried, purified, and stored to manufacture valuable industrial products, such as biofuels
425 and plastic [67]. The 786 kg calcined carbonated HCP produced during the CO₂ release
426 stage can be used as a cementitious material in concrete, as mentioned previously. With
427 such a technology roadmap, 210 kg of CO₂ can be captured and utilized from concrete

428 demolition wastes, and 786 kg of valuable calcined carbonated HCP can be collected
429 for concrete production in a recycling phase, which is somewhat efficient and
430 ecofriendly.

431

432 4.3. Life cycle assessment (LCA) for producing 1 t calcined carbonated HCP–OPC 433 mixtures

434 A typical “cradle-to-grave” LCA was conducted according to the International
435 Organization for Standards 14040 (ISO 14040) [68]. In this study, the CML 2002
436 approach, one of the most widely used methodologies, was used to evaluate and
437 compare the environmental impacts of producing 1 ton of M20 and OPC pastes [68].

438

439 4.3.1. Goal, scope, and system boundary

440 The system boundary covers raw material production to the final product packing
441 [69]. Two materials, that is, plain OPC paste and calcined carbonated HCP–OPC paste,
442 were adopted to compare their environmental impacts. M20 (80 wt.% OPC and 20 wt.%
443 calcined carbonated HCP with a W/CM ratio of 0.4) and OPC paste (100 wt.% OPC
444 with a W/CM ratio of 0.4) were selected. M20 was chosen for the LCA because it
445 exhibited the best strength performance among the three mixtures with different
446 replacement ratios. The functional unit of the LCA was 1 t of M20 and OPC pastes
447 under the same curing conditions (Table 5). The process flow diagrams for the M20 and
448 OPC pastes are shown in Fig. 9, where the dashed lines represent the system boundaries
449 for both materials. Before analysis, some assumptions were made. 1) The transportation

450 and use phases might have environmental impacts, although these two phases were
451 assumed to be the same with the various types of concrete. 2) All OPC pastes used to
452 produce the M20 and OPC pastes were obtained from Europe for consistency. 3)
453 Because the demolished concrete could be derived entirely from the waste, the
454 environmental impacts caused by recycling demolished concrete were neglected in this
455 LCA; however, the CCUS technology for manufacturing calcined carbonated HCP
456 should be considered. The CCUS technology process can be considered a roadmap (Fig.
457 8).

458

459 4.3.2. Inventory

460 For the LCA, inventory data for the raw materials and processing procedures
461 were acquired from the Ecoinvent database and existing literature [70] [71] [72] [73]
462 [74] [75]. The details of the raw materials used for manufacturing the M20 and OPC
463 pastes are described below.

464 The OPC produced from the clinker and gypsum was set as CEM I 42.5 N-type
465 cement. Boesch and Hellweg reported life-cycle impact assessment (LCIA) results for
466 cement production in Europe [76]. Hence, the detailed OPC production processes,
467 including crushing, milling, blending, and calcination, are not described in this paper
468 [73]. The environmental impact data for tap water were collected directly from the
469 Ecoinvent database. The production of calcined carbonated HCP powder is complicated
470 because of its CCUS process, which consists of crushing and screening HCP from
471 demolished waste, sequestering CO₂ in HCP, and calcining carbonated HCP. The

472 environmental impacts of the crushing and milling phases are explained in *Table of*
473 *Bond Work Index by Minerals*¹. Mercante et al. [75] reported the energy and material
474 input for sorting and recycling mixed construction and demolition waste (concrete), in
475 which diesel fuel, electrical energy, and water accounted for 1.02 L, 2.59 kWh, and 1.00
476 L, respectively, for 1 t waste. Owing to the limited research on recycling HCP from
477 demolition waste, the life cycle inventory of HCP collection was performed for the
478 recycled aggregate production, as reported in [77] [78] [79] [80]. HCP carbonation
479 requires gas pressure. As mentioned above, CO₂ gas pressure of 1.5 MPa was applied
480 for carbonation. Therefore, the LCIA data for carbonation were used as compressed air
481 with an average generation of <30 kW 12 bar gauge according to the Ecoinvent database.
482 The required CO₂ volume for HCP carbonation to produce 143 kg of calcined
483 carbonated HCP was calculated based on the experimentally used autoclave. Based on
484 the experimental results for the weight change ratio and TGA for the HCP, carbonated
485 HCP, and calcined carbonated HCP, 220 kg of carbonated HCP and 174 kg of HCP were
486 required. Typically, HCP accounts for 25 wt.% in concrete; therefore, the estimated total
487 weight of demolished concrete was 696 kg [81]. Considering the time required for
488 carbonation to reach equilibrium (the gas pressure inside the chamber does not change
489 with time), the required CO₂ volume for HCP carbonation was 3.08 m³. Finally, the
490 calcination of carbonated HCP (also called CO₂ separation) was conducted at 1000 °C,
491 but the actual decomposition temperature of CaCO₃ generally ranged from 500 to

¹ Table of Bond Work Index by Minerals: <https://www.911metallurgist.com/blog/table-of-bond-work-index-by-minerals>

492 900 °C, as measured using TGA. Therefore, it was assumed that the starting temperature
493 was room temperature, and CaCO₃ decomposition was completed at 900 °C. The
494 calcination process for converting calcium carbonates into CaO is the most energy-
495 intensive stage [82]. Giordano et al. [83] reported in detail the LCA of postcombustion
496 CO₂ capture, in which the LCIA of CO₂ separation related to natural gas combustion in
497 an auxiliary gas turbine (functional unit of per ton CO₂) was used to calculate the
498 environmental impacts of the calcination phase of the proposed CCUS roadmap. Based
499 on the above discussion, the LCIA of the CCUS technology in the proposed roadmap
500 is presented in Table 6.

501

502 4.3.3. Impact assessment of M20 and OPC paste production

503 Five baseline categories were adopted to estimate the environmental impacts of
504 producing M20 and OPC pastes. These categories are global warming potential (GWP),
505 ozone depletion potential (ODP), photochemical ozone creation potential (POCP),
506 acidification potential (AP), and eutrophication potential (EP) [84]. The functional units
507 of GWP, ODP, POCP, AP, and EP are kg CO₂-eq., kg CFC-11-eq., kg C₂H₄-eq., kg SO₂-
508 eq., and kg PO₄³⁻-eq., respectively.

509 Based on this classification, the impact assessment of the raw materials used for
510 producing M20 and plain OPC paste and the total environmental impact were
511 determined (Table 7). Cement production in manufacturing 1 t of M20 and OPC paste
512 was dominant in GWP, ODP, POCP, AP, and EP. For the OPC paste, water production
513 generally had no significant impact in these five categories, and the highest degree of

514 the environmental impact of water production was 1.21% for ODP. For M20, calcined
515 carbonated HCP production may result in high greenhouse gas emissions. However,
516 because of the lower amount of calcined carbonated HCP in M20, the environmental
517 impact of HCP calcination (3.63%) was significantly lower than that of cement
518 production (96.35%) in GWP. The most significant effect of the calcined carbonated
519 HCP was observed for the ODP, which accounted for 16.35% of the total impact. The
520 difference ratios of LCIA for the GWP, ODP, POCP, AP, and EP between these two
521 materials were calculated as $(LCIA_{M20} - LCIA_{OPC\ paste})/LCIA_{OPC\ paste}$ (Table 7) to
522 compare the environmental impacts of M20 and OPC pastes. The results showed that
523 the total environmental impacts of producing 1 t of M20 were less severe than those of
524 OPC paste, particularly for EP, which decreased by up to 17.7%. Thus, calcined
525 carbonated HCPs satisfy the required mechanical properties of construction materials
526 and are ecofriendlier than conventional cement-based materials.

527

528 4.4. Limitations of CCUS technology

529 Although the CO₂ transport routine from the emission source to the reuse in
530 bioproduct manufacture was qualitatively and quantitatively clarified in the proposed
531 technology route. Calcination of carbonated HCP for releasing captured CO₂ is still not
532 an ideal method because of the non-negligible energy consumption. In future studies,
533 the release of CO₂ from carbonated HCP without calcination should be further
534 investigated. If solved, the CaL technique can also be improved. However, CCUS
535 technology still faces various penalties and limitations, such as energy consumption,

536 financial needs, and public awareness. [85] [86]. Leonzio et al. [85] reported a net
537 present value of 0.554 trillion euros and a payback period of 2.85 years for the best
538 CCUS supply chain. Saito et al. [87] conducted a survey to assess the current status of
539 general public awareness and opinion on CCUS in Japan. They observed a somewhat
540 low level of climate change consciousness and a passive attitude toward CCUS policies.
541 Moreover, two cases of CO₂ storage are discussed, demonstrating the restrictions of
542 CCUS in many countries. The CO₂-EOR project in Gao 89 is a CO₂ geological storage
543 project in China. CO₂ injection and storage were analyzed by Ma et al. [88]. Four CO₂
544 gas wells, that is, Gao 89-4, Gao 89-5, Gao 89-16, and Gao 89-17, were selected to
545 calculate the accumulated amount of CO₂ injected and generated. A total of 62,000 tons
546 of CO₂ was injected, and a total of 58634.71 tons of CO₂ was stored underground by
547 the end of 2011. During this process, investment in the project cannot be ignored. Such
548 techniques for reducing and storing anthropogenic CO₂ are limited and significantly
549 less effective than expected. Another example is the multicriteria analysis conducted by
550 Vögele et al., which evaluated the feasibility of CCUS in Germany [11]. They compared
551 the possible impacts of deploying CCUS in six scenarios (REF, REF_high, CCS,
552 CCS_high, REG, and REG_high), which differed in renewables and certificate prices.
553 The results indicate a gloomy future for the CCUS technology in Germany. Because of
554 the overall cost of the electricity supply system and the cost sensitivity to changes in
555 the CO₂ allowance, several disadvantages exist in the operation phase of the electricity
556 supply equipped with CCUS technology. The uncertainties in the feasibility of this
557 technique account for a higher risk, hindering CCUS development. Governmental

558 regulations regarding CCUS may raise companies' unwillingness to apply CCUS.
559 Hence, simultaneously achieving economy, energy conservation, and public acceptance
560 is still a considerable task for researchers and workers in CCUS.

561

562 **5. Conclusions**

563

564 In this study, the phase compositions of calcined carbonated HCP and the effect
565 of calcined carbonated HCP powders on the performance of OPC-based pastes were
566 investigated. Calcined carbonated HCP was manufactured using HCPs subjected to
567 carbonation and calcination. Various tests, including the compressive strength test,
568 XRD, TGA, and FTIR, were performed. An LCA was then conducted to evaluate and
569 compare the environmental impacts of producing 1 t of M20 and OPC pastes. The
570 following conclusions were drawn.

571 (1) Based on the TGA results, HCP carbonation significantly consumed portlandite
572 to form calcium carbonates, with a CO₂ uptake ratio of 21.61%. C-S-H in the HCP
573 generally remained noncarbonated, which may be attributed to the newly formed calcite,
574 preventing further gaseous CO₂ penetration.

575 (2) The calcination of carbonated HCP decomposed the main nanocrystal phase of
576 C-S-H and the crystal phases of portlandite and various calcium carbonates, forming
577 lime and wollastonite.

578 (3) At the same W/CM ratio of 0.4, the partial replacement of calcined carbonated
579 HCP increased the 28-day compressive strength by up to 8%, with an optimum

580 replacement ratio of 20%. This was because of the filler effect of wollastonite and the
581 early-age strength improvement effect of lime; above the optimum replacement ratio,
582 the strength significantly decreased because of the dilution effect.

583 (4) Based on the microscopic characterizations, the major crystal phases in calcined
584 carbonated HCP – OPC pastes were identified, including C-S-H, portlandite,
585 monocarboaluminate, and some calcium carbonates formed by natural carbonation. The
586 crystal phases generally remained unchanged with an increasing replacement ratio of
587 calcined carbonated HCP.

588 (5) Finally, a conceptual technology roadmap for CCUS adopting HCP was
589 proposed. In addition, the LCA impacts of producing 1 t of M20 were less severe than
590 those of plain OPC paste in the five environmental impact categories (GWP, ODP,
591 POCP, AP, and EP). This study provides a reference for applying demolition waste in
592 CCUS and concrete production.

593

594 **Conflict of interest**

595 The authors declare that there is no conflict of interest.

596

597 **Data availability statement**

598 Some or all data, models, and codes that support the findings of this study are
599 available from the corresponding author upon reasonable request.

600

601 **Tables**

602 Table 1. Chemical compositions of OPC by mass (wt.%).

Component	Cement
CaO	63.57
SiO ₂	20.58
Al ₂ O ₃	4.97
Fe ₂ O ₃	3.76
SO ₃	2.00
MgO	2.29
f-CaO	0.75
Na ₂ O _{eq}	0.53
LOI	1.40

603

604 Table 2. Mixing proportions.

Mixture ID	OPC/g	HCP- calcination/g	Water/g	Total weight/g	Replacement ratio/%
Ref.	42.86	0			0
M10	38.57	4.29	17.14	60	10
M20	34.29	8.57			20
M30	30.00	12.86			30

605

606 Table 3. Details of samples at each processing stage.

Sample	Content	Processing procedure	Weight/g *		Weight change ratio/%
			Before	After	
HCP	Fully hydrated cement paste	Hydrated for 3 months at 60 ± 0.5 °C	-	-	-
HCP- carbonation	Carbonated HCP	Carbonation for 24 hours at constant gas pressure of 1.5 MPa and constant temperature of 60 ± 0.5 °C	120.0	145.5	21.25
HCP- calcination	Calcined HCP- carbonation	Calcination at 1000 °C	135.8	87.8	35.35

607 *Weights of samples before and after processing are listed in the fourth and fifth
 608 columns, respectively. These abbreviations were also used in the figures.

609

610 Table 4. Quantification of water and CO₂ contents calculated using TGA.

Mix	Weight loss percentage (%)					
	30-300 °C	300-500 °C	500-900 °C	H ₂ O	CO ₂	Total
Ref.	9.02	5.76	6.65	14.78	6.65	21.43
M10	9.31	5.75	6.08	15.06	6.08	21.14
M20	9.37	5.94	5.92	15.31	5.92	21.23
M30	9.71	6.40	6.65	16.11	6.65	22.76

611

612 Table 5. Production of 1 t M20 and OPC paste.

Raw materials	OPC cement/kg	HCP- calcination /kg	Water/kg
M20	572	143	285
OPC paste	715	0	285

613

614 Table 6. Environmental impacts of producing 143 kg calcined HCP.

Procedure	GWP/kg CO ₂ -eq.	ODP/kg CFC-11-eq.	POCP/kg C ₂ H ₄ -eq.	AP/kg SO ₂ -eq.	EP/kg PO ₄ ³⁻ -eq.
Crushing and screening	8.004	1.559×10 ⁻⁶	2.847×10 ⁻³	0.056	3.605×10 ⁻³
Carbon capture	0.010	3.883×10 ⁻¹³	4.231×10 ⁻⁷	3.125×10 ⁻⁴	8.690×10 ⁻⁹
Calcination	11.448	9.850×10 ⁻⁷	5.220×10 ⁻⁴	6.490×10 ⁻³	1.130×10 ⁻³
Total environmental impacts	19.462	2.544×10 ⁻⁶	3.369×10 ⁻³	0.0630	4.735×10 ⁻³

615

616 Table 7. Environmental impacts of producing 1 t M20 and OPC paste.

Materials	Mixture type	GWP/kg CO ₂ -eq.	ODP/kg CFC-11-eq.	POCP/kg C ₂ H ₄ -eq.	AP/kg SO ₂ -eq.	EP/kg PO ₄ ³⁻ -eq.
OPC	M20	516.516	1.282×10 ⁻⁵	0.024	1.293	0.168
	OPC paste	645.645	1.602×10 ⁻⁵	0.030	1.616	0.210

Water	M20	0.122	1.967×10^{-7}	2.327×10^{-12}	2.454×10^{-5}	6.505×10^{-9}
	OPC paste	0.122	1.967×10^{-7}	2.327×10^{-12}	2.454×10^{-5}	6.505×10^{-9}
HCP- calcination	M20	19.462	2.544×10^{-6}	3.369×10^{-3}	0.0630	4.735×10^{-3}
	OPC paste	0	0	0	0	0
Total environmental impacts	M20	536.101	1.556×10^{-5}	0.027	1.356	0.173
	OPC paste	645.767	1.622×10^{-5}	0.030	1.616	0.210
Difference ratio (%)		-17.0	-4.1	-8.8	-16.1	-17.7

617

618

619 **References**

620

- 621 [1] E. Benhelal, G. Zahedi, E. Shamsaei, A. Bahadori, Global strategies and potentials
622 to curb CO₂ emissions in cement industry, *J. Clean. Prod.* 51 (2013) 142-161.
623 <https://doi.org/10.1016/j.jclepro.2012.10.049>.
- 624 [2] C. Chen, G. Habert, Y. Bouzidi, A. Jullien, Environmental impact of cement
625 production: Detail of the different processes and cement plant variability
626 evaluation, *J. Clean. Prod.* 18 (2010) 478-485.
627 <https://doi.org/10.1016/j.jclepro.2009.12.014b>.
- 628 [3] J. Li, L. Spanu, J. Heo, W. Zhang, D.W. Gardner, C. Carraro, R. Maboudian, P.J.M.
629 Monteiro, Sequestration of solid carbon in concrete: A large-scale enabler of
630 lower-carbon intensity hydrogen from natural gas, *MRS Bull.* 46 (8) (2021)
631 680-686. <https://doi.org/10.1557/s43577-021-00118-z>.
- 632 [4] X.F. Zhang, S.Y. Zhang, Z.Y. Hu, G. Yu, C.H. Pei, R.N. Sa, Identification of
633 connection units with high ghg emissions for low-carbon product structure
634 design, *J. Clean. Prod.* 27 (2012) 118-125.
635 <https://doi.org/10.1016/j.jclepro.2012.01.011>.
- 636 [5] K.L. Scrivener, V.M. John, E.M. Gartner, Eco-efficient cements: Potential
637 economically viable solutions for a low- CO₂ cement-based materials industry,
638 *Cem. Concr. Res.* 114 (2018) 2-26.
639 <https://doi.org/10.1016/j.cemconres.2018.03.015>.
- 640 [6] J. Skocek, M. Zajac, M. Ben Haha, Carbon capture and utilization by mineralization
641 of cement pastes derived from recycled concrete, *Sci. Rep.* 10 (1) (2020) 5614.
642 <https://doi.org/10.1038/s41598-020-62503-z>.
- 643 [7] C. Ridtirud, C. Prinya, Influences of the ratios of high-calcium fly ash to low-
644 calcium fly ash on the strength and drying shrinkage of geopolymer mortar, *Adv.*
645 *Mater. Res.* 931-932 (2014) 416-420.
646 <https://doi.org/10.4028/www.scientific.net/AMR.931-932.416>.
- 647 [8] L.A. Qureshi, B. Ali, A. Ali, Combined effects of supplementary cementitious
648 materials (silica fume, GGBS, fly ash and rice husk ash) and steel fiber on the
649 hardened properties of recycled aggregate concrete, *Constr. Build. Mater.* 263
650 (2020) 120636. <https://doi.org/10.1016/j.conbuildmat.2020.120636>.
- 651 [9] F.M. Baena-Moreno, M. Rodríguez-Galán, F. Vega, B. Alonso-Fariñas, L.F. Vilches
652 Arenas, B. Navarrete, Carbon capture and utilization technologies: A literature
653 review and recent advances, *Energ. Sources. A* 41 (12) (2019) 1403-1433.
654 <https://doi.org/10.1080/15567036.2018.1548518>.
- 655 [10] R. Zevenhoven, J. Fagerlund, J.K. Songok, CO₂ mineral sequestration:
656 Developments toward large-scale application, *Greenhouse Gases: Sci. Technol.*
657 1 (1) (2011) 48-57. <https://doi.org/10.1002/ghg3.7>.
- 658 [11] S. Vögele, D. Rübhelke, P. Mayer, W. Kuckshinrichs, Germany's "no" to carbon
659 capture and storage: Just a question of lacking acceptance?, *Appl. Energy* 214
660 (2018) 205-218. <https://doi.org/10.1016/j.apenergy.2018.01.077>.

- 661 [12] B. Šavija, M. Luković, Carbonation of cement paste: Understanding, challenges,
 662 and opportunities, *Constr. Build. Mater.* 117 (2016) 285-301.
 663 <https://doi.org/10.1016/j.conbuildmat.2016.04.138>.
- 664 [13] S. Ruan, C. Unluer, Influence of mix design on the carbonation, mechanical
 665 properties and microstructure of reactive mgo cement-based concrete, *Cem.*
 666 *Concr. Compos.* 80 (2017) 104-114.
 667 <https://doi.org/10.1016/j.cemconcomp.2017.03.004>.
- 668 [14] E.R. Bobicki, Q. Liu, Z. Xu, H. Zeng, Carbon capture and storage using alkaline
 669 industrial wastes, *Prog. Energy Combust. Sci.* 38(2) (2012) 302-320.
- 670 [15] N.D. Oikonomou, Recycled concrete aggregates, *Cem. Concr. Compos.* 27 (2)
 671 (2005) 315-318. <https://doi.org/10.1016/j.cemconcomp.2004.02.020>.
- 672 [16] P.H.R. Borges, J.O. Costa, N.B. Milestone, C.J. Lynsdale, R.E. Streatfield,
 673 Carbonation of CH and C-S-H in composite cement pastes containing high
 674 amounts of BFS, *Cem. Concr. Res.* 40 (2) (2010) 284-292.
 675 <https://doi.org/10.1016/j.cemconres.2009.10.020>.
- 676 [17] L. Wang, J. Wang, X. Qian, P. Chen, Y. Xu, J. Guo, An environmentally friendly
 677 method to improve the quality of recycled concrete aggregates, *Constr. Build.*
 678 *Mater.* 144 (2017) 432-441. <https://doi.org/10.1016/j.conbuildmat.2017.03.191>.
- 679 [18] M. Zajac, J. Skocek, J. Skibsted, M. Ben Haha, CO₂ mineralization of demolished
 680 concrete wastes into a supplementary cementitious material – a new CCU
 681 approach for the cement industry, *RILEM Technical Letters* 6 (0) (2021) 53-60.
 682 <https://doi.org/10.21809/rilemtechlett.2021.141>.
- 683 [19] M. Zajac, J. Skocek, P. Durdzinski, F. Bullerjahn, J. Skibsted, M. Ben Haha, Effect
 684 of carbonated cement paste on composite cement hydration and performance,
 685 *Cem. Concr. Res.* 134 (2020) 106090.
 686 <https://doi.org/10.1016/j.cemconres.2020.106090>.
- 687 [20] S. Ortabay, J. Li, G. Geng, R. Myers, P. Monteiro, R. Maboudian, C. Carraro,
 688 Effects of CO₂ and temperature on the structure and chemistry of C-(A-)S-H
 689 investigated by Raman spectroscopy, *RSC Adv.* 7 (2017) 48925-48933.
 690 <https://doi.org/10.1039/C7RA07266J>.
- 691 [21] M. Fernández Bertos, S.J.R. Simons, C.D. Hills, P.J. Carey, A review of accelerated
 692 carbonation technology in the treatment of cement-based materials and
 693 sequestration of CO₂, *J. Hazard. Mater.* 112 (3) (2004) 193-205.
 694 <https://doi.org/10.1016/j.jhazmat.2004.04.019>.
- 695 [22] B. Lu, C. Shi, J. Zhang, J. Wang, Effects of carbonated hardened cement paste
 696 powder on hydration and microstructure of portland cement, *Constr. Build.*
 697 *Mater.* 186 (2018) 699-708. <https://doi.org/10.1016/j.conbuildmat.2018.07.159>.
- 698 [23] L. Liu, Y. Ji, F. Gao, L. Zhang, Z. Zhang, X. Liu, Study on high-efficiency CO₂
 699 absorption by fresh cement paste, *Constr. Build. Mater.* (2020) 121364.
 700 <https://doi.org/10.1016/j.conbuildmat.2020.121364>.
- 701 [24] R. Hay, J. Li, K. Celik, Phase evolution, micromechanical properties, and
 702 morphology of calcium (alumino)silicate hydrates C-(A-)S-H under
 703 carbonation, *Cem. Concr. Res.* 152 (2022) 106683.
 704 <https://doi.org/10.1016/j.cemconres.2021.106683>.

- 705 [25] Y. Wang, S. Y. Lin, Y. Suzuki., Limestone calcination with CO₂ capture (I),
706 decomposition behavior in a CO₂ atmosphere, *Energy Fuels* 21 (2007) 3317-
707 3321. <https://doi.org/10.1021/ef700318c>.
- 708 [26] C. Ortiz, J.M. Valverde, R. Chacartegui, L.A. Perez-Maqueda, P. Giménez, The
709 calcium-looping (CaCO₃/CaO) process for thermochemical energy storage in
710 concentrating solar power plants, *Renew. Sustain. Energy Rev.* 113 (2019)
711 109252. <https://doi.org/10.1016/j.rser.2019.109252>.
- 712 [27] G. Colelli, R. Chacartegui, C. Ortiz, A. Carro, A.P. Arena, V. Verda, Life cycle and
713 environmental assessment of calcium looping (CaL) in solar thermochemical
714 energy storage, *Energ. Convers. Manage.* 257 (2022) 115428.
715 <https://doi.org/10.1016/j.enconman.2022.115428>.
- 716 [28] S. Lin, T. Kiga, Y. Wang, K. Nakayama, Energy analysis of CaCO₃ calcination with
717 CO₂ capture, *Energy Procedia* 4 (2011) 356-361.
718 <https://doi.org/10.1016/j.egypro.2011.01.062>.
- 719 [29] Z.C. Wang, Q. Bai, G. Dresen, R. Wirth, B. Evans, High-temperature deformation
720 of calcite single crystals, *J. Geophys. Res. Solid Earth* 101 (B9) (1996) 20377-
721 20390. <https://doi.org/10.1029/96jb01186>.
- 722 [30] S.K. Das, S.M. Mustakim, A. Adesina, J. Mishra, T.S. Alomayri, H.S. Assaedi, C.R.
723 Kaze, Fresh, strength and microstructure properties of geopolymer concrete
724 incorporating lime and silica fume as replacement of fly ash, *J. Build. Eng.* 32
725 (2020) 101780. <https://doi.org/10.1016/j.jobe.2020.101780>.
- 726 [31] J. Li, Q. Jin, W. Zhang, C. Li, P.J.M. Monteiro, Microstructure and durability
727 performance of sustainable cementitious composites containing high-volume
728 regenerative biosilica, *Resour. Conserv. Recycl.* 178 (2022) 106038.
729 <https://doi.org/10.1016/j.resconrec.2021.106038>.
- 730 [32] H. Mehdizadeh, E. Najafi Kani, A. Palomo Sanchez, A. Fernandez-Jimenez,
731 Rheology of activated phosphorus slag with lime and alkaline salts, *Cem. Concr.*
732 *Res.* 113 (2018) 121-129. <https://doi.org/10.1016/j.cemconres.2018.07.010>.
- 733 [33] M. Mazloom, A.A. Ramezani-pour, J.J. Brooks, Effect of silica fume on
734 mechanical properties of high-strength concrete, *Cem. Concr. Compos.* 26 (4)
735 (2004) 347-357. [https://doi.org/10.1016/S0958-9465\(03\)00017-9](https://doi.org/10.1016/S0958-9465(03)00017-9).
- 736 [34] S.A. Barbhuiya, J.K. Gbagbo, M.I. Russell, P.A.M. Basheer, Properties of fly ash
737 concrete modified with hydrated lime and silica fume, *Constr. Build. Mater.* 23
738 (10) (2009) 3233-3239. <https://doi.org/10.1016/j.conbuildmat.2009.06.001>.
- 739 [35] Y.K. Kong, Y. Song, K. Kurumisawa, T. Wang, D. Yan, Q. Zeng, X. Zhou, S. Ruan,
740 Use of hydrated cement pastes (HCP) as a CO₂ sponge, *J. CO₂ Util.* 55 (2022)
741 101804. <https://doi.org/10.1016/j.jcou.2021.101804>.
- 742 [36] C. Unluer, A. Al-Tabbaa, Impact of hydrated magnesium carbonate additives on
743 the carbonation of reactive mgo cements, *Cem. Concr. Res.* 54 (2013) 87-97.
744 <https://doi.org/10.1016/j.cemconres.2013.08.009>.
- 745 [37] ASTM C150/C150M-20, Standard specification for Portland cement, ASTM
746 International, West Conshohocken, PA (2020).

- 747 [38] C. Shi, Y. Li, J. Zhang, W. Li, L. Chong, Z. Xie, Performance enhancement of
 748 recycled concrete aggregate – a review, *J. Clean. Prod.* 112 (2016) 466-472.
 749 <https://doi.org/10.1016/j.jclepro.2015.08.057>.
- 750 [39] A. Carriço, J.A. Bogas, S. Hu, S. Real, M.F. Costa Pereira, Novel separation
 751 process for obtaining recycled cement and high-quality recycled sand from
 752 waste hardened concrete, *J. Clean. Prod.* 309 (2021) 127375.
 753 <https://doi.org/10.1016/j.jclepro.2021.127375>.
- 754 [40] ASTM C305, Standard practice for mechanical mixing of hydraulic cement pastes
 755 and mortars of plastic consistency, ASTM International, PA (2020).
- 756 [41] B. Lothenbach, T. Matschei, G. Möschner, F. Glasser, Thermodynamic modeling
 757 of the effect of temperature on the hydration and porosity of portland cement,
 758 *Cem. Concr. Res.* 38 (2008) 1-18.
 759 <https://doi.org/10.1016/j.cemconres.2007.08.017>.
- 760 [42] T. Wang, H. Huang, X. Hu, M. Fang, Z. Luo, R. Guo, Accelerated mineral
 761 carbonation curing of cement paste for CO₂ sequestration and enhanced
 762 properties of blended calcium silicate, *Chemical Engineering Journal* 323 (2017)
 763 320-329. <https://doi.org/10.1016/j.cej.2017.03.157>.
- 764 [43] ASTM C109/C109M-20b, Standard test method for compressive strength of
 765 hydraulic cement mortars (using 2-in. or [50 mm] cube specimens), ASTM
 766 International, West Conshohocken, PA (2020).
- 767 [44] H. Ye, L. Huang, Degradation mechanisms of alkali-activated binders in sulfuric
 768 acid: The role of calcium and aluminum availability, *Constr. Build. Mater.* 246
 769 (2020) 118477. <https://doi.org/10.1016/j.conbuildmat.2020.118477>.
- 770 [45] J.L. Provis, A. Palomo, C. Shi, Advances in understanding alkali-activated
 771 materials, *Cem. Concr. Res.* 78 (2015) 110-125.
 772 <https://doi.org/10.1016/j.cemconres.2015.04.013>.
- 773 [46] R. Snellings, G. Mertens, J. Elsen, Supplementary cementitious materials, *Rev.*
 774 *Mineral. Geochem.* 74 (2012) 211-278. <https://doi.org/10.2138/rmg.2012.74.6>.
- 775 [47] M. Liu, S. Hong, Y. Wang, J. Zhang, D. Hou, B. Dong, Compositions and
 776 microstructures of hardened cement paste with carbonation curing and further
 777 water curing, *Constr. Build. Mater.* 267 (2021) 121724.
 778 <https://doi.org/10.1016/j.conbuildmat.2020.121724>.
- 779 [48] R. Guo, Q. Chen, H. Huang, X. Hu, T. Wang, Carbonation curing of industrial solid
 780 waste-based aerated concretes, *Greenhouse Gases: Sci. Technol.* 9 (4) (2019)
 781 <https://doi.org/10.1002/ghg.1862>.
- 782 [49] X. Pan, C. Shi, X. Hu, Z. Ou, Effects of CO₂ surface treatment on strength and
 783 permeability of one-day-aged cement mortar, *Constr. Build. Mater.* 154 (2017)
 784 1087-1095. <https://doi.org/10.1016/j.conbuildmat.2017.07.216>.
- 785 [50] J. Li, W. Zhang, P.J.M. Monteiro, Synchrotron x-ray Raman scattering shows the
 786 changes of the Ca environment in C-S-H exposed to high pressure, *Cem. Concr.*
 787 *Res.* 132 (2020) 106066. <https://doi.org/10.1016/j.cemconres.2020.106066>.
- 788 [51] R.-S. Lin, Y. Han, X.-Y. Wang, Macro-meso-micro experimental studies of
 789 calcined clay limestone cement (LC3) paste subjected to elevated temperature,

- 790 Cem. Concr. Compos. 116 (2021) 103871.
 791 <https://doi.org/10.1016/j.cemconcomp.2020.103871>.
- 792 [52] B. Xu, B. Lothenbach, F. Winnefeld, Influence of wollastonite on hydration and
 793 properties of magnesium potassium phosphate cements, *Cem. Concr. Res.* 131
 794 (2020) 106012. <https://doi.org/10.1016/j.cemconres.2020.106012>.
- 795 [53] R.I. Khan, W. Ashraf, Effects of ground wollastonite on cement hydration kinetics
 796 and strength development, *Constr. Build. Mater.* 218 (2019) 150-161.
 797 <https://doi.org/10.1016/j.conbuildmat.2019.05.061>.
- 798 [54] K. Traoré, T.S. Kabré, P. Blanchart, Gehlenite and anorthite crystallisation from
 799 kaolinite and calcite mix, *Ceram. Intl.* 29 (4) (2003) 377-383.
 800 [https://doi.org/10.1016/S0272-8842\(02\)00148-7](https://doi.org/10.1016/S0272-8842(02)00148-7).
- 801 [55] R. Hay, K. Celik, Accelerated carbonation of reactive magnesium oxide cement
 802 (rmc)-based composite with supercritical carbon dioxide (scCO₂), *J. Clean.*
 803 *Prod.* 248 (2020) 119282. <https://doi.org/10.1016/j.jclepro.2019.119282>.
- 804 [56] G. Ye, X. Liu, G. De Schutter, A.M. Poppe, L. Taerwe, Influence of limestone
 805 powder used as filler in SCC on hydration and microstructure of cement pastes,
 806 *Cem. Concr. Compos.* 29 (2) (2007) 94-102.
 807 <https://doi.org/10.1016/j.cemconcomp.2006.09.003>.
- 808 [57] M. Abdel Wahab, I. Abdel Latif, M. Kohail, A. Almasry, The use of wollastonite
 809 to enhance the mechanical properties of mortar mixes, *Constr. Build. Mater.* 152
 810 (2017) 304-309. <https://doi.org/10.1016/j.conbuildmat.2017.07.005>.
- 811 [58] P. Kalla, A. Rana, Y.B. Chad, A. Misra, L. Csetenyi, Durability studies on concrete
 812 containing wollastonite, *J. Clean. Prod.* 87 (2015) 726-734.
 813 <https://doi.org/10.1016/j.jclepro.2014.10.038>.
- 814 [59] W.A. Gutteridge, J.A. Dalziel, Filler cement: The effect of the secondary
 815 component on the hydration of portland cement: Part I. A fine non-hydraulic
 816 filler, *Cem. Concr. Res.* 20 (5) (1990) 778-782. [https://doi.org/10.1016/0008-8846\(90\)90011-L](https://doi.org/10.1016/0008-8846(90)90011-L).
- 818 [60] Y. Briki, M. Zajac, M.B. Haha, K. Scrivener, Impact of limestone fineness on
 819 cement hydration at early age, *Cem. Concr. Res.* 147 (2021) 106515.
 820 <https://doi.org/10.1016/j.cemconres.2021.106515>.
- 821 [61] P. He, C. Shi, Z. Tu, C.S. Poon, J. Zhang, Effect of further water curing on
 822 compressive strength and microstructure of CO₂-cured concrete, *Cem. Concr.*
 823 *Compos.* 72 (2016) 80-88. <https://doi.org/10.1016/j.cemconcomp.2016.05.026>.
- 824 [62] Z. Tian, H. Ye, Electrical resistivity of partially-saturated alkali-activated slag
 825 containing sodium nitrite admixture, *Cem. Concr. Compos.* 120 (2021) 104053.
 826 <https://doi.org/10.1016/j.cemconcomp.2021.104053>.
- 827 [63] W. Ashraf, J. Olek, Carbonation behavior of hydraulic and non-hydraulic calcium
 828 silicates: Potential of utilizing low-lime calcium silicates in cement-based
 829 materials, *J. Mater. Sci.* 51 (13) (2016) 6173-6191.
 830 <https://doi.org/10.1007/s10853-016-9909-4>.
- 831 [64] K. Kobayashi, K. Suzuki, Y. Uno, Carbonation of concrete structures and
 832 decomposition of C-S-H, *Cem. Concr. Res.* 24 (1) (1994) 55-61.
 833 [https://doi.org/10.1016/0008-8846\(94\)90082-5](https://doi.org/10.1016/0008-8846(94)90082-5).

- 834 [65] P.J.M. Monteiro, G. Geng, D. Marchon, J. Li, P. Alapati, K.E. Kurtis, M.J.A. Qomi,
835 Advances in characterizing and understanding the microstructure of
836 cementitious materials, *Cem. Concr. Res.* 124 (2019) 105806.
837 <https://doi.org/10.1016/j.cemconres.2019.105806>.
- 838 [66] IPCC, Fourth assessment report (AR4), Working Group I, UNEP, New York, 2007.
- 839 [67] C. Andrade, M.Á. Sanjuán, Updating carbon storage capacity of Spanish cements,
840 *Sustainability* 10 (12) (2018) 4806. <https://www.mdpi.com/2071-1050/10/12/4806>.
841
- 842 [68] L.C. Dreyer, A.L. Niemann, M.Z. Hauschild, Comparison of three different lca
843 methods: EDIP97, CML2001 and Eco-indicator 99, *Int. J. Life Cycle Asses.* 8
844 (4) (2003) 191-200. <https://doi.org/10.1007/BF02978471>.
- 845 [69] J.B. Guinée, E. Lindeijer, Handbook on life cycle assessment: Operational guide
846 to the ISO standards, Dordrecht: Kluwer Academic Publishers; 2002.
- 847 [70] R. Lacy, M. Molina, M. Vaca, C. Serralde, G. Hernandez, G. Rios, E. Guzman, R.
848 Hernandez, R. Perez, Life-cycle ghg assessment of carbon capture, use and
849 geological storage (CCUS) for linked primary energy and electricity production,
850 *Int. J. Greenhouse Gas Ctrl.* 42 (2015) 165-174.
851 <https://doi.org/10.1016/j.ijggc.2015.07.017>.
- 852 [71] E. Batuecas, F. Liendo, T. Tommasi, S. Bensaid, F.A. Deorsola, D. Fino, Recycling
853 CO₂ from flue gas for CaCO₃ nanoparticles production as cement filler: A life
854 cycle assessment, *J. CO₂ Util.* 45 (2021) 101446.
855 <https://doi.org/10.1016/j.jcou.2021.101446>.
- 856 [72] S. Ruan, C. Unluer, Comparative life cycle assessment of reactive MgO and
857 Portland cement production, *J. Clean. Prod.* 137 (2016) 258-273.
858 <https://doi.org/10.1016/j.jclepro.2016.07.071>.
- 859 [73] D. Huntzinger, T. Eatmon, A life-cycle assessment of Portland cement
860 manufacturing: Comparing the traditional process with alternative technologies,
861 *J. Clean. Prod.* 17 (2009) 668-675.
862 <https://doi.org/10.1016/j.jclepro.2008.04.007>.
- 863 [74] T. Stengel, P. Schießl, 22 - life cycle assessment (lca) of ultra high performance
864 concrete (uhpc) structures, in: F. Pacheco-Torgal, L.F. Cabeza, J. Labrincha, A.
865 de Magalhães (Eds.), *Eco-efficient construction and building materials*,
866 Woodhead Publishing 2014, pp. 528-564.
- 867 [75] I.T. Mercante, M.D. Bovea, V. Ibáñez-Forés, A.P. Arena, Life cycle assessment of
868 construction and demolition waste management systems: A Spanish case study,
869 *Int. J. Life Cycle Asses.* 17 (2) (2012) 232-241. <https://doi.org/10.1007/s11367-011-0350-2>.
870
- 871 [76] M.E. Boesch, S. Hellweg, Identifying improvement potentials in cement
872 production with life cycle assessment, *Environ. Sci. Technol.* 44 (23) (2010)
873 9143-9149. <https://doi.org/10.1021/es100771k>.
- 874 [77] L. Caneda-Martínez, M. Monasterio, J. Moreno-Juez, S. Martínez-Ramírez, R.
875 García, M. Frías, Behaviour and properties of eco-cement pastes elaborated with
876 recycled concrete powder from construction and demolition wastes, *Mater.* 14
877 (5) (2021) 1299. <https://www.mdpi.com/1996-1944/14/5/1299>.

- 878 [78] S.-M. Jian, B. Wu, N. Hu, Environmental impacts of three waste concrete recycling
879 strategies for prefabricated components through comparative life cycle
880 assessment, *J. Clean. Prod.* 328 (2021) 129463.
881 <https://doi.org/10.1016/j.jclepro.2021.129463>.
- 882 [79] W. Xing, V.W.Y. Tam, K.N. Le, J.L. Hao, J. Wang, Life cycle assessment of
883 recycled aggregate concrete on its environmental impacts: A critical review,
884 *Constr. Build. Mater.* 317 (2022) 125950.
885 <https://doi.org/10.1016/j.conbuildmat.2021.125950>.
- 886 [80] R. Kurda, J.D. Silvestre, J. de Brito, Life cycle assessment of concrete made with
887 high volume of recycled concrete aggregates and fly ash, *Resour. Conserv.
888 Recycl.* 139 (2018) 407-417. <https://doi.org/10.1016/j.resconrec.2018.07.004>.
- 889 [81] S.H. Chu, Y.K. Kong, Mathematical model for strength of alkali-activated
890 materials, *J. Build. Eng.* 44 (2021) 103189.
891 <https://doi.org/10.1016/j.jobe.2021.103189>.
- 892 [82] T. Wang, D.-C. Xiao, C.-H. Huang, Y.-K. Hsieh, C.-S. Tan, C.-F. Wang, CO₂ uptake
893 performance and life cycle assessment of cao-based sorbents prepared from
894 waste oyster shells blended with pmma nanosphere scaffolds, *J. Hazard. Mater.*
895 270 (2014) 92-101. <https://doi.org/10.1016/j.jhazmat.2014.01.026>.
- 896 [83] L. Giordano, D. Roizard, E. Favre, Life cycle assessment of post-combustion CO₂
897 capture: A comparison between membrane separation and chemical absorption
898 processes, *Int. J. Greenhouse Gas Ctrl.* 68 (2018) 146-163.
899 <https://doi.org/10.1016/j.ijggc.2017.11.008>.
- 900 [84] P. Van den Heede, N. De Belie, Environmental impact and life cycle assessment
901 (LCA) of traditional and 'green' concretes: Literature review and theoretical
902 calculations, *Cem. Concr. Compos.* 34 (4) (2012) 431-442.
903 <https://doi.org/10.1016/j.cemconcomp.2012.01.004>.
- 904 [85] G. Leonzio, D. Bogle, P.U. Foscolo, E. Zondervan, Optimization of CCUS supply
905 chains in the UK: A strategic role for emissions reduction, *Chem. Eng. Res. Des.*
906 155 (2020) 211-228. <https://doi.org/10.1016/j.cherd.2020.01.002>.
- 907 [86] Q. Li, Z.A. Chen, J.T. Zhang, L.C. Liu, X.C. Li, L. Jia, Positioning and revision of
908 CCUS technology development in china, *Int. J. Greenhouse Gas Ctrl.* 46 (2016)
909 282-293. <https://doi.org/10.1016/j.ijggc.2015.02.024>.
- 910 [87] A. Saito, K. Itaoka, M. Akai, Those who care about ccs—results from a Japanese
911 survey on public understanding of CCS, *Int. J. Greenhouse Gas Ctrl.* 84 (2019)
912 121-130. <https://doi.org/10.1016/j.ijggc.2019.02.014>.
- 913 [88] J. Ma, Y. Yang, H. Wang, L. Li, Z. Wang, D. Li, How much CO₂ is stored and
914 verified through CCS/CCUS in China?, *Energy Procedia* 154 (2018) 60-65.
915 <https://doi.org/10.1016/j.egypro.2018.11.011>.

916

917 **List of Figures**

918 Fig. 1. XRD patterns of HCP, HCP-carbonation and HCP-calcination.

919 Fig. 2. TG and DTG curves of HCP, HCP-carbonation and HCP-calcination.

920 Fig. 3. Compressive strength results.

921 Fig. 4. XRD patterns of paste samples.

922 Fig. 5. TG and DTG curves of paste samples.

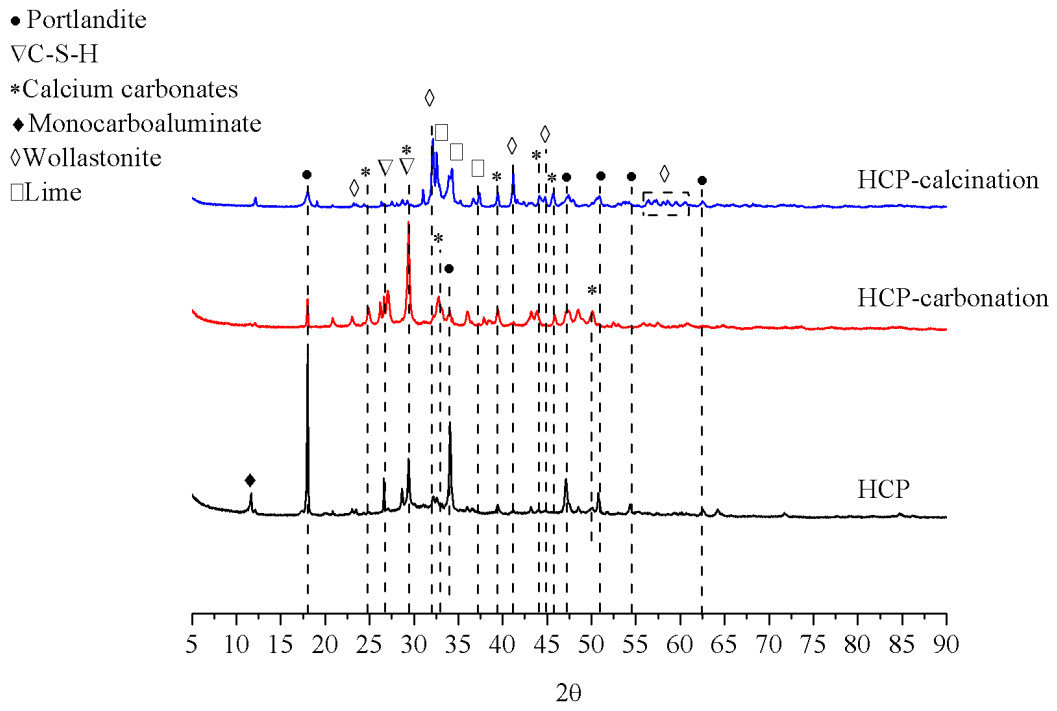
923 Fig. 6. FTIR spectra of paste samples.

924 Fig. 7. Hydration behaviors of HCP-calcination-OPC pastes.

925 Fig. 8. Technology roadmap for CCUS using demolition waste.

926 Fig. 9. The process and system boundaries of 1 tonne (a) M20 production and (b) OPC
927 paste production.

928

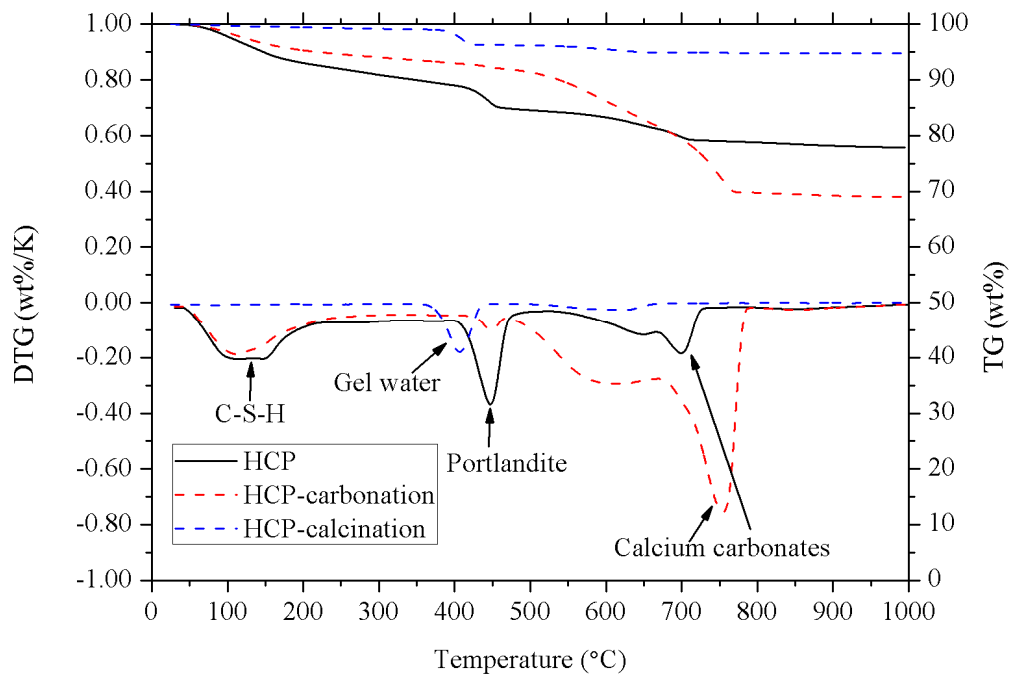


929

930

Fig. 1. XRD patterns of HCP, HCP-carbonation and HCP-calcination.

931

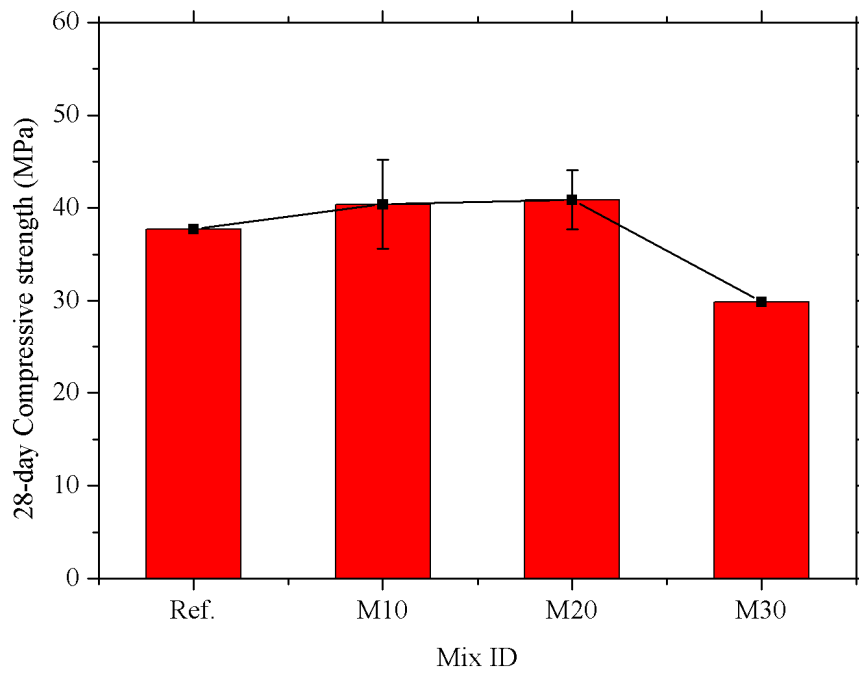


932

933

Fig. 2. TG and DTG curves of HCP, HCP-carbonation and HCP-calcination.

934



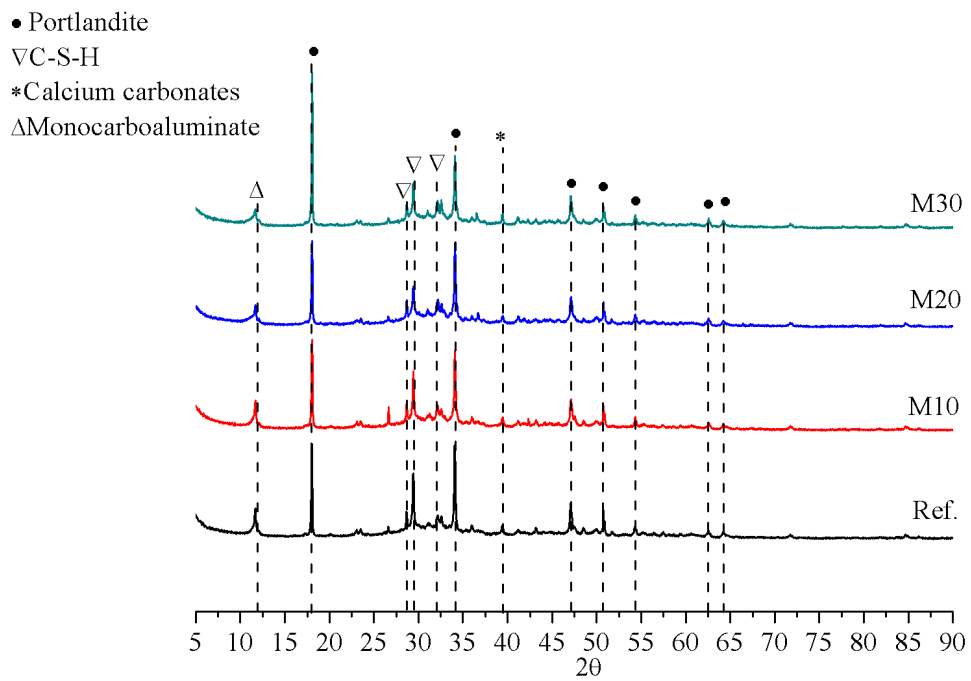
935

936

Fig. 3. Compressive strength results.

937

938



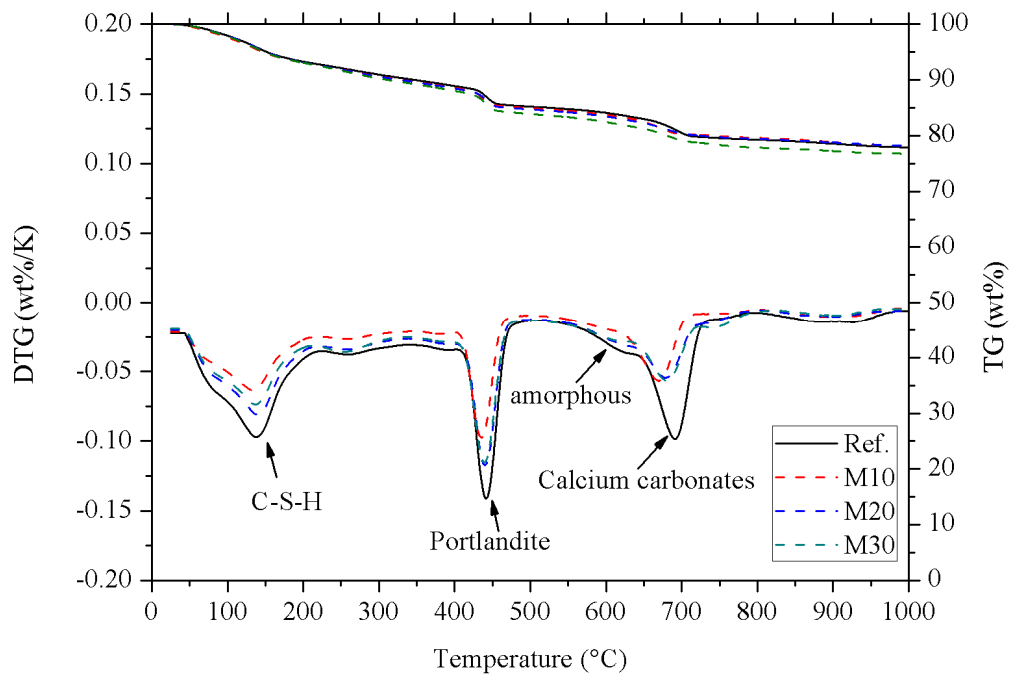
939

940

Fig. 4. XRD patterns of paste samples.

941

942

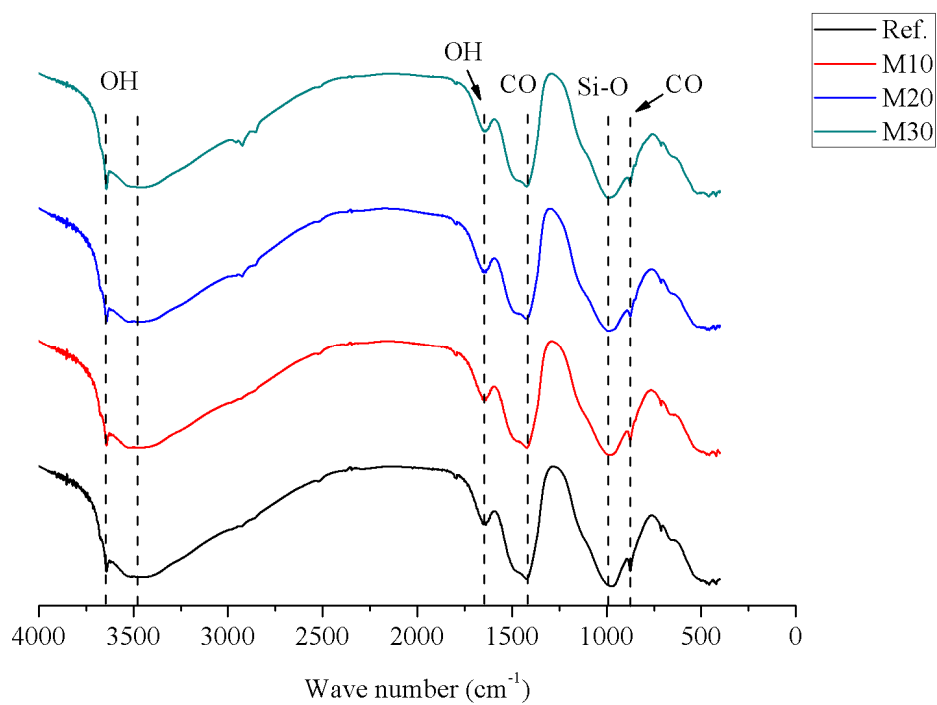


943

944

Fig. 5. TG and DTG curves of paste samples.

945



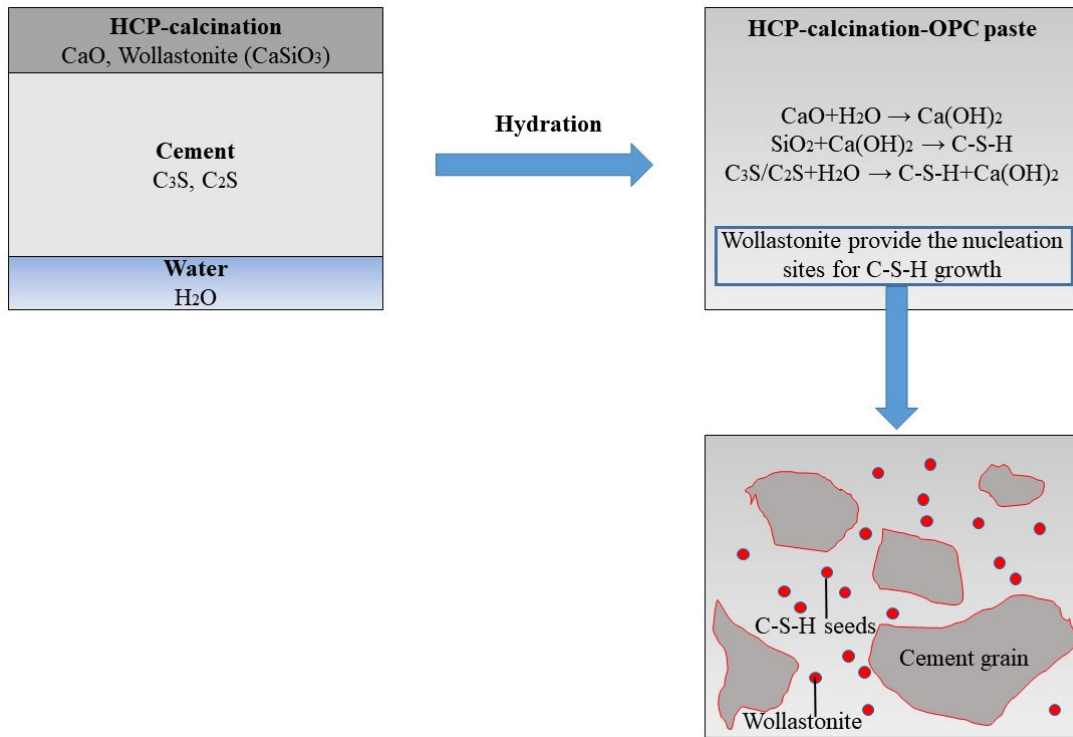
946

947

Fig. 6. FTIR spectra of paste samples.

948

949



950

951

Fig. 7. Hydration behaviors of HCP-calcination-OPC pastes.

952

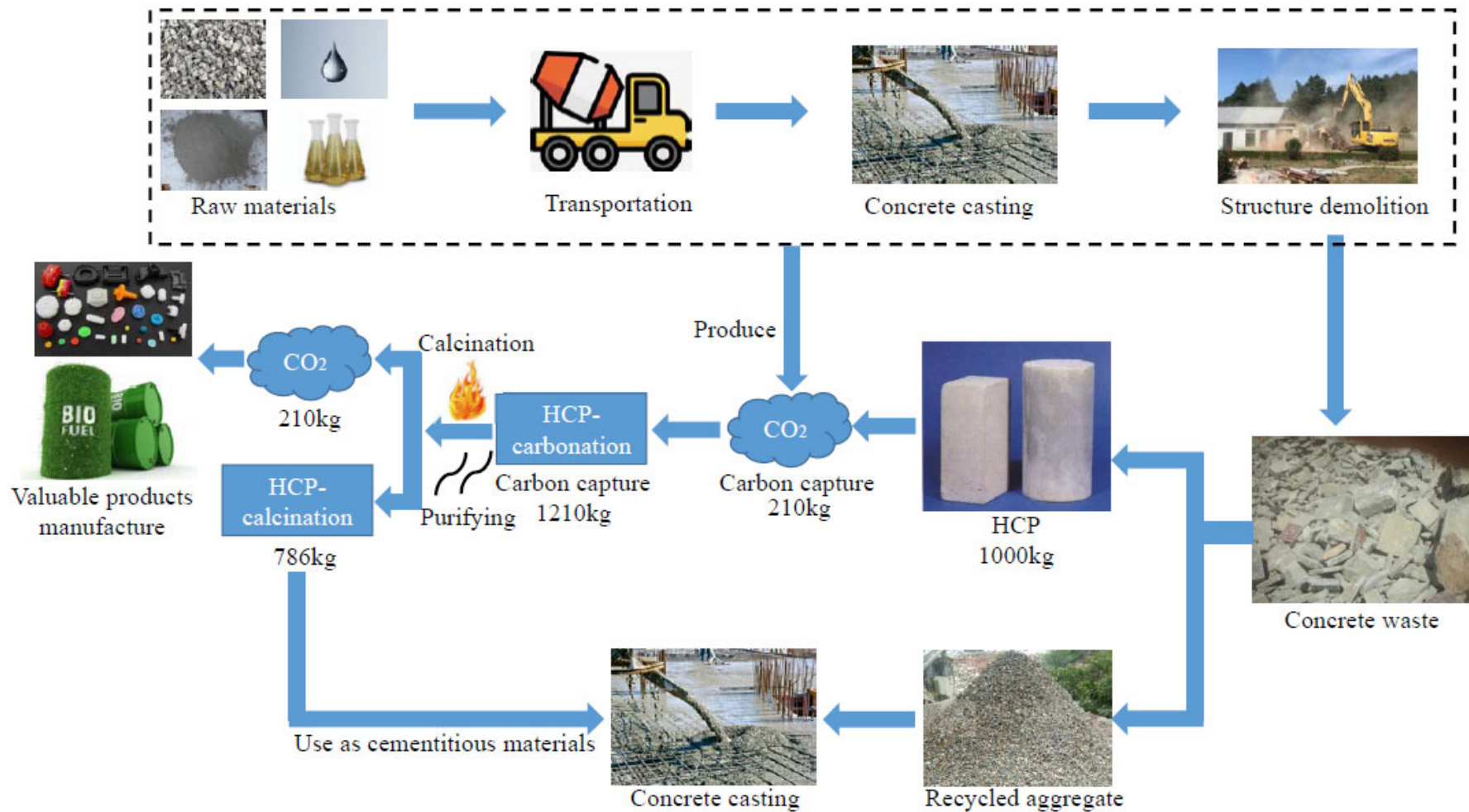
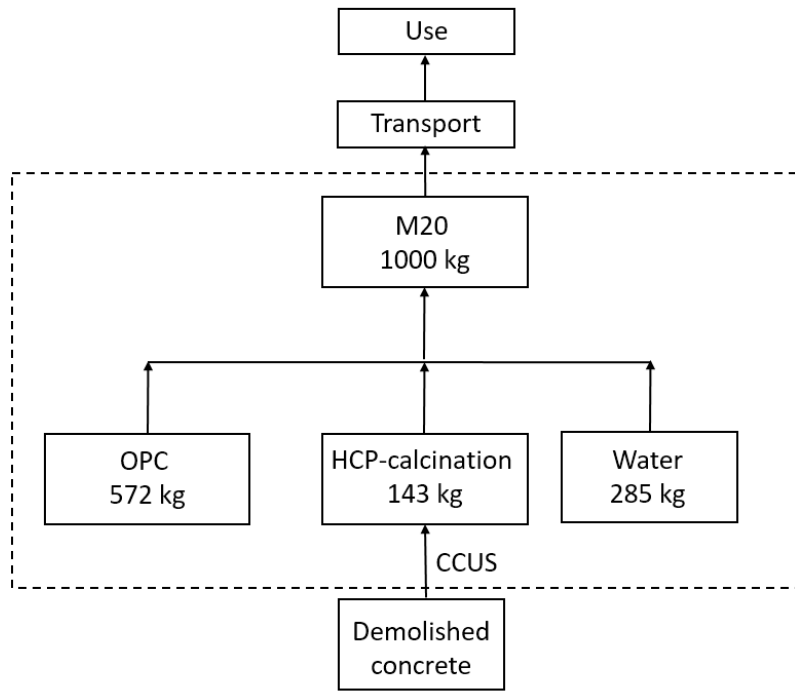


Fig. 8. Technology roadmap for CCUS using demolition waste

953

954

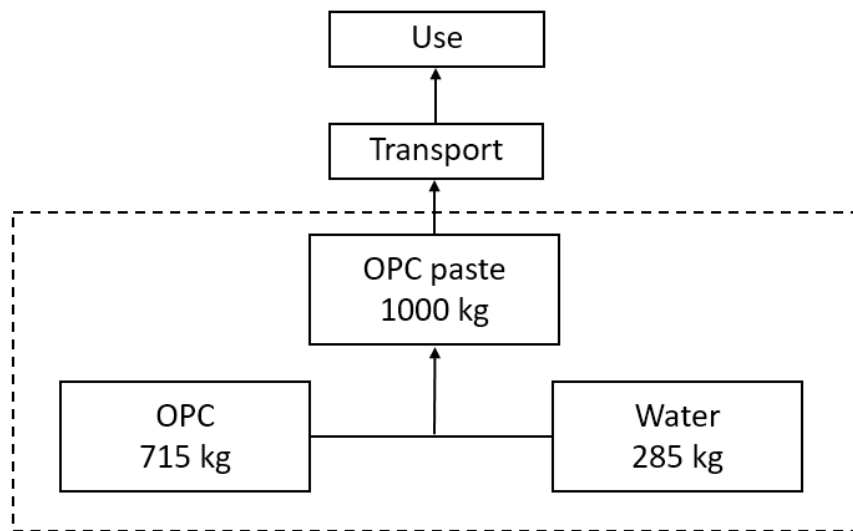
955



956

957

(a)



958

959

(b)

960

Fig. 9. The process and system boundaries of 1 tonne (a) M20 production and (b)

961

OPC paste production.

